VOL. 11, NO. 14, JULY 2016 ISSN 1819-6608
ARPN Journal of Engineering and Applied Sciences

www.arpnjournals.com

EFFECT OF INJECTION ON THERMAL AND FLOW CHARACTERISTICS OF COPPER MHD NANOFLUID IN THE PRESENCE OF SEA WATER/FRESH WATER

E. N. Ashwin Kumar[1], Norasikin Mat Isa[1], B. Vibhu Vignesh[1] and R. Kandasamy[2]
[1]Mechanical and Manufacturing Engineering, FKMP, UTHM, Malaysia
[2]Computational Fluid Dynamics, FSSW, UTHM, Malaysia
E-Mail: ashwinkumaren@gmail.com

ABSTRACT

In this paper, we analyse the steady stagnation-point flow and heat transfer of an incompressible copper nanofluids towards a shrinking/stretching surface. Copper nanoparticles of volume fraction 0.2% are dispersed in fresh water and sea water. The governing Navier-Stokes' partial differential equations are transformed to a set of nonlinear ordinary differential equations by means of a similarity transformation. The nonlinear equations are then solved numerically by using Runge-Kutta-Fehlberg method with shooting technique. A comparison analyses on sea water/fresh water based copper nanofluids is presented to investigate the effect of injection under the influence of pertinent parameters such as the magnetic parameter, Grashof number, Eckert number, thermal radiation and heat generation are discussed over a vertical porous surface. The temperature and velocity distributions of nanofluids at the porous surface illustrates that both nanofluids have quite similar characteristics for all stream conditions. Comparisons with published results is presented.

Keywords: sea water/fresh water based copper nanofluid, stagnation–point flow, stretching/shrinking porous surface, similarity transformation, thermal radiation and heat source.

INTRODUCTION

Natural convective heat transfer plays a vital role in engineering systems because of its wide applications in cooling condenser of buildings, solar heating, defense and space applications, and thermal systems. The heat transfer performance in such systems is important from the industrial and energy saving prospects. The conventional heat transfer fluids, such as water, acetone and ethylene glycol have very low thermal conductivity which is disadvantage in improving the heat transfer characteristics and the compactness of such thermal systems. Choi [1], introduced a new approach by using particles in nano-meter (10^{-9}) scale dispersed in a conventional fluids, known as nanofluid has been studied extensively in recent years [2], [3] in major applications. Free convection heat transfer study using nanofluids has gained high interests and there are projects undergoing throughout the world on the effect of nanoparticles on heat transfer enhancement in natural convective applications. Few Examples are the results obtained by [4] who studied Cu–water nanofluids in a 2-D rectangular enclosure and stated that an enhancement in heat transfer with an increase in volume fraction of the suspended nanoparticles at any given Grashof number.

Oztop and Abu-Nada [5] presented similar results, where an increase in heat transfers was observed by the addition of nanoparticles. Hamad and Ferdows [7] investigated the boundary layer flow of electrically conducting fluid and heat transfer over a shrinking surface. They studied different types of nanoparticles and found each nanoparticle differed from others in physical characteristics each possess different character. They enclosed that changing the nanoparticle type, changed the behaviour of the fluid flow.

Mahapatra and Gupta [8] observed the heat transfer in stagnation-point flow towards a stretching plate. The governing system of PDE was converted to ODE by using similarity transformations, then evaluated using the Keller-box method. The study was to understand the effects of the governing parameters, namely the suction/injection parameter, Prandtl number on the velocity and temperature profiles. MHD stagnation-point flow and boundary layer flow is studied by [9], [10] over a stretching surface. According to their results, it is clear that when stretching velocity is lower than that of free stream velocity, there is an increase in velocity at one point with an increase in magnetic field.

Owing to the need of replacement of fresh water and other conventional heat transfer fluids, researches are carried all over the world to use sea water as coolant. Cooling of condensers using sea water in buildings situated near sea. Andersen [6], investigated that by using sea water, energy used for generation of cooling can be saved up to up to 30%. Proper understanding of the behaviour of sea water as coolant will be of great benefit in general. The physical properties of seawater include both thermodynamic properties' like density and freezing point, as well as 'transport properties' like the electrical conductivity and viscosity. Pawlowicz [11] stated that density is usually calculated using a mathematical function of temperature, salinity, and pressure, sometimes called an equation of state. Sharqawy [12] calculated thermo-physical properties by changing temperature and salinity.

The objective of the present work is to study the stagnation-point flow and heat transfer characteristic of copper nanofluids of Pal [13]. In this paper, we investigate the behaviour of velocity and temperature profiles of sea water/fresh water based copper nanofluids in the presence of magnetic field, thermal radiation, heat source, Grashof

number and Eckert number in the presence of injection on the stretching/shrinking wall.

NOMENCLATURE

Symbol	Quantity	units
B_0	Magnetic field strength	N/Am
Cu	Copper	
C_p	Specify heat of solid	m^2/s^2K
Ec	Eckert number	Nil
$f'(\eta)$	Velocity	Nil
Gr	Grashof number	Nil
g	Gravitational force	m/s^2
K_1	Permeability of the porous medium	m^2
K*	Mean spectral absorption coefficient	1/m
M	Magnetic field strength parameter	$Nm/\Omega A^2 s^1$
MHD	Magnetohydrodynamics	N
N	Thermal radiation parameter	$s3/m^2$
ODE	Ordinary differential equations	Nil
PDE	Partial differential equations	Nil
Pr	Prandtl number	Nil
Q_o	Heat generation/absorption coefficient	$kg/m^1s^3K^1$
Re	Reynolds number	Nil
S	Injection velocity parameter	Nil
T	Temperature	K
u, v	Velocity components in x,y-directions respectively	m/s
u_w	Stretching or shrinking surface velocity	m/s
U	Free stream velocity of the nanofluid	m/s
2-D	Two dimensional	Nil
Greek letters		
α	Thermal diffusivity	m^2/s
β	Thermal expansion coefficient	1/K
Γ	Buoyancy parameter	Nil
η	Similarity variable	Nil
$\theta(\eta)$	temperature of the fluid	Nil
θ_w	Wall temperature excess ratio parameter	Nil
$\theta'(\eta)$	heat transfer rate	Nil
κ	Thermal conductivity	kgm/s^3K
λ	Heat sink/source parameter	Nil
μ	Dynamic viscosity	kg/ms
ρ	Density	kg/m^3
ρC_p	Heat capacitance	J/m^3K
σ	Electrical conductivity	$1/\Omega m$
σ^*	Stefan–Boltzmann constant	kg/m^2K^4
Φ	Nanoparticles volume fraction	vol%
ψ	Stream function	m^2/s
Subscripts		
nf	Nanofluid	
f	Fluid	
s	Solid	

MATHEMATICAL ANALYSIS

The flow model for achieving our objectives is shown in Figure-1. In this study, the nanofluid flow is selected to be a 2-D stagnation-point flow, over a permeable plate. The plate is subjected to shrinking and stretching; for stretching plate the linear velocity over a porous plate is $u_w = cx$ and the velocity over a porous plate becomes negative for shrinking plate that is $u_w = -cx$. The flow is time independent and laminar flow. $U(x) = ax$ is defined as the free stream flow. Magnetic field strength (B_0) which is present in positive x-axis, influences the nanofluid flow. Nanoparticles and base fluids are assumed to be in thermal equilibrium and no slip occurs between them. The acceleration due to gravity is denoted by g. The thermo-physical properties of base fluid and nanoparticle is given in Table-1. Prandtl number of fresh water is taken as 6.2 at 20℃. Sea water with Pr =7.155 at 20℃, salinity = 35 °/oo.

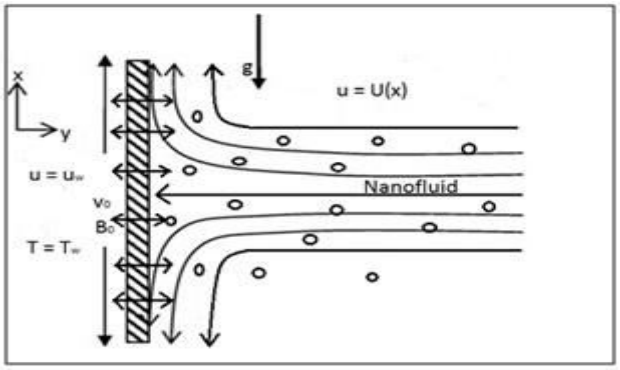

Figure-1. Stagnation-point flow model over a vertical permeable plate.

Table-1. Thermo-physical properties of fluid and copper nanoparticle. [5], [12].

Physical properties	Fresh water at 20℃	Sea water at 20℃ (Salinity=35g/kg)	Cu
C_p	4179	4000	385
ρ	997.1	1025	8933
κ	0.613	0.6015	401

With above assumptions, the boundary layer equations are as follows:

$$\frac{\partial u}{\partial x}+\frac{\partial v}{\partial y}=0 \tag{1}$$

$$u\frac{\partial u}{\partial x}+v\frac{\partial v}{\partial y}=U(x)\frac{dU(x)}{dx}+\frac{\mu_{nf}}{\rho_{nf}}\frac{\partial^2 u}{\partial y^2}+\frac{\mu_{nf}}{\rho_{nf}K}(U(x)-u) \tag{2}$$

$$u\frac{\partial T}{\partial x}+v\frac{\partial T}{\partial y}=\alpha_{nf}\frac{d^2T}{dy^2}+\frac{Q_0}{(\rho C_p)_{nf}}(T-T_\infty)-\frac{1}{(\rho C_p)_{nf}}\frac{\partial q_r}{\partial y}+\frac{\mu_{nf}}{(\rho C_p)_{nf}}\left(\frac{\partial u}{\partial y}\right)^2 \tag{3}$$

Subjected to the boundary conditions (for shrinking or stretching plate)

$$v=v_0, u=u_w(x)=\pm cx, T=T_w \text{ at } y=0;\quad T\to T_\infty, u\to U(x)=ax, C\to C_\infty \text{ as } y\to\infty \tag{4}$$

For calculating density, thermal conductivity, dynamic viscosity, thermal diffusivity and heat capacitance of nanofluids the below mentioned equations are used.

$$\rho_{nf}=(1-\phi)\rho_f+\phi\rho_s \tag{5}$$

$$\kappa_{nf}=\kappa_f\left[\frac{\kappa_s+2\kappa_f-2\phi(\kappa_s-\kappa_f)}{\kappa_s+2\kappa_f+2\phi(\kappa_s-\kappa_f)}\right] \tag{6}$$

$$\mu_{nf}=\frac{\mu_f}{(1-\phi)^{2.5}} \tag{7}$$

$$(\rho C_p)_{nf}=(1-\phi)(\rho C_p)_f+\phi(\rho C_p)_s \tag{8}$$

$$\alpha_{nf}=\frac{\kappa_{nf}}{(\rho C_p)_{nf}} \tag{9}$$

Equation. (1) to Equation. (3) is transformed using similarity functions, the stream function are

$$\psi=\sqrt{c\cdot\nu_f}\cdot f(\eta)\cdot x,\quad \eta=\sqrt{\frac{c}{\nu_f}}\cdot y,\quad (T_w-T_\infty)\,\theta(\eta)=T-T_\infty \tag{10}$$

$$\theta_w=\frac{T_w}{T_\infty} \tag{11}$$

Defining the stream function ψ that is, (u) = ψ_y, (v) = $-\psi_x$, which satisfies the Equation. (1) and Equation. (5) to Equation. (9) are substituted into Equation. (2), Equation. (3) and Equation. (4), we get following non-linear ODE:

$$f'''+((1-\phi)^{2.5}M+K)\left(\frac{a}{c}-f'\right)+(1-\phi)^{2.5}\left(1-\phi+\phi\frac{\rho_s}{\rho_f}\right)\left(\frac{a^2}{c^2}+ff''-f'^2+\gamma\theta\right)=0 \tag{12}$$

$$\theta''+\frac{Pr}{\left(\frac{\kappa_{nf}}{\kappa_f}+N(1+(\theta_w-1)\theta)^3\right)}\cdot\left[\frac{3N}{Pr}\cdot(\theta_w-1)(1+(\theta_w-1)\theta)^2\theta'^2+\left(1-\phi+\phi\frac{(\rho C_p)_s}{(\rho C_p)_f}\right)(F\theta'-2F'\theta)+\lambda\theta\right]+\frac{Ec}{(1-\phi)^{2.5}}\theta'=0 \tag{13}$$

Boundary conditions for stretching and shrinking plate:

$$\left.\begin{array}{l} f=S, f'=1, \theta=1 \text{ at } \eta=0 \text{ (stretching)} \\ f=S, f'=-1, \theta=1 \text{ at } \eta=0 \text{ (shrinking)} \\ f'\to\frac{a}{c}, \theta\to 0, \ \eta\to\infty \end{array}\right\} \text{ as } y=0 \tag{14}$$

$Pr=\frac{\nu}{\alpha}$ is the Prandtl number, $Ec=\frac{u_w{}^2}{C_p\Delta T}$ is the Eckerts number, $Gr=\frac{g\beta(T_w-T_\infty)x^3}{\nu^2}$ is the Grashof number, $\gamma=\frac{Gr}{Re^2}$ is the Buoyancy parameter, $S=-\frac{v_w}{\sqrt{c\nu_f}}$ is the injection parameter, $\lambda=\frac{Q_0\nu_f}{c\kappa_{nf}}$ is the heat source/sink, $K=\frac{\nu_f}{cK_1}$ is the porous parameter, $N=\frac{16\sigma^*T_f{}^3}{3k_fK^*}$ is the thermal radiation parameter and $M=\frac{\sigma B_0^2}{\rho_f c}$ is the magnetic parameter.

Table-2. Comparison of –θ'(0) obtained from MAPLE software with published works for stretching plate.

Pr	a/c	[9]	[14]	Present results
1	0.1	0.625	0.6216	0.62537
	1	0.796	0.8001	0.79967
	2	1.124	1.1221	1.12375
1.5	0.1	0.797	0.7952	0.79500
	1	0.974	0.7952	0.79503
	2	1.341	1.3419	1.34095

For validating the results obtained from MAPLE 18 software, the values for the parameters as given in previously presented journals by [9], [13], [14] are given in MAPLE 18 software to obtain heat transfer rate values and velocity profiles. From Table-2., the dimensionless heat transfer rates obtained from MAPLE 18 software is in agreement with previously published journals by [9], [14]. From Figure-2 and Figure-3., the velocity profiles obtained in MAPLE 18 software is in perfect correlation with that of results of [13].

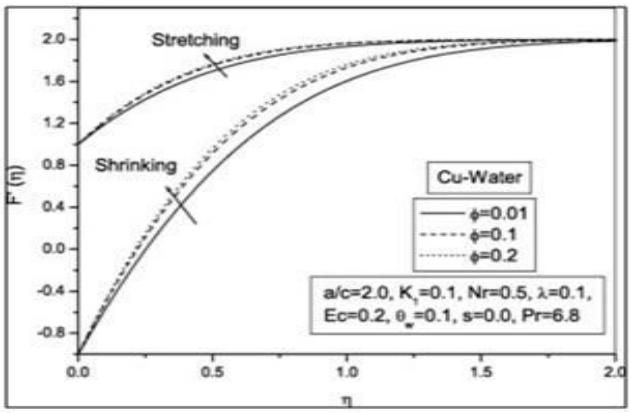

Figure-2. Nanoparticle volume fraction effect on copper nanofluid [13].

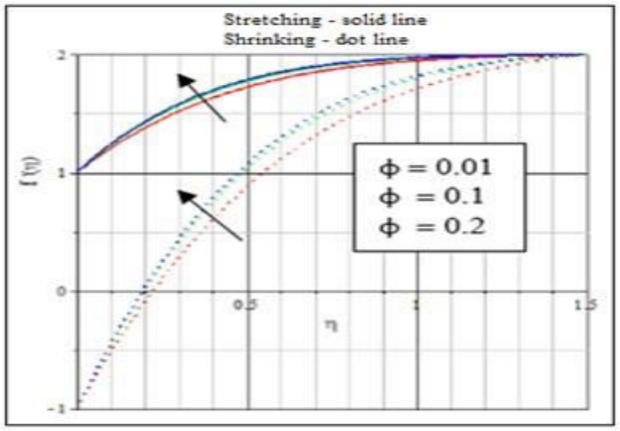

Figure-3. Nanoparticle volume fraction effect on copper nanofluid (MAPLE 18 software).

RESULT AND DISCUSSION

The set of equations (12) and (13) is highly nonlinear. Hence coupled and cannot be solved analytically and numerical solutions subject to the boundary conditions (14) are obtained using the very robust computer algebra software Maple 18. This software uses a fourth-fifth order Runge–Kutta–Fehlberg method as default to solve boundary value problems numerically using the dsolve command. The transformed system of coupled nonlinear ordinary differential Equations (12) and (13) including boundary conditions (14) depend on the various parameters.

The increase in thermal conductivity of copper nanofluids for increase in nanoparticle volume fraction (ϕ) is shown in Table-3. Thermal conductivity is calculated using (6) which is relative to ϕ and assuming the nanoparticle to be spherical in shape. When compared between the thermal conductivity enhancements of Cu-sea water and Cu-fresh water, it is evident that the thermal conductivities in case of Cu-sea water is lesser than the Cu-fresh water.

Figure-4 and Figure-5., present the velocity profiles for Cu-sea water and Cu-fresh water in the presence of injection velocities for different values of Magnetic parameter (M). In shrinking surfaces, when the nanofluid flow come closer to the momentum boundary layer, as the difference in magnitude is so thin and $\eta < 0.3$ for injection, similar velocity profiles for increase in M. In the presence of injection, velocity distribution decreases for increase in M. The order of magnitude of variation in the velocity profiles is greater in the case of suction velocity than in the case of injection. The effects of M in decelerating the flow by opposing force known as Lorentz force. This is the reason for high magnitude variation in velocity profiles, between suction and injection velocity profiles. Figure-4 and Figure-5., in both cases, Cu-sea water nanofluid has less velocity than the Cu-fresh water nanofluid. The order of magnitude in variation among the velocity profiles is very less between the nanofluids.

Table-3. Thermal conductivity (κ) of nanofluids for different nanoparticle volume fraction (ϕ).

Nanoparticle volume fraction (ϕ) (vol%)	Thermal conductivity (κ)			
	Fresh water	Sea water	Cu-fresh water	Cu-sea water
0	0.613	0.6015	0.613	0.6015
0.1	0.613	0.6015	0.9177	0.9006
0.2	0.613	0.6015	1.4241	1.3975
0.3	0.613	0.6015	2.4311	2.3858
0.4	0.613	0.6015	5.4066	5.3071

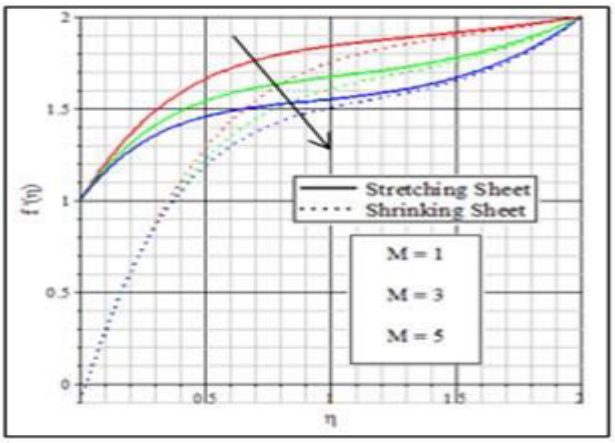

Figure-4. Magnetic effects on velocity profiles over Cu-sea water (Pr =6.2, ϕ=0.2, Gr=3, K = 0.1, S = -1, λ = 0.1, N =1,Ec=0.2)

Figure-6 and Figure-7, temperatures profiles for Cu-sea water and Cu-fresh water in the presence of injection for different values of magnetic field parameter (M) is analyzed. The temperature distribution is higher in case of shrinking than stretching surfaces. In the presence of injection, it is observed that the thermal boundary layer thickness of shrinking surface is significantly stronger than that of stretching surface. In the presence of injection, it is noticed that the temperature of Cu-sea water decreases near the boundary layer and then increases with increase

of M for shrinking surface whereas it increases for stretching street.

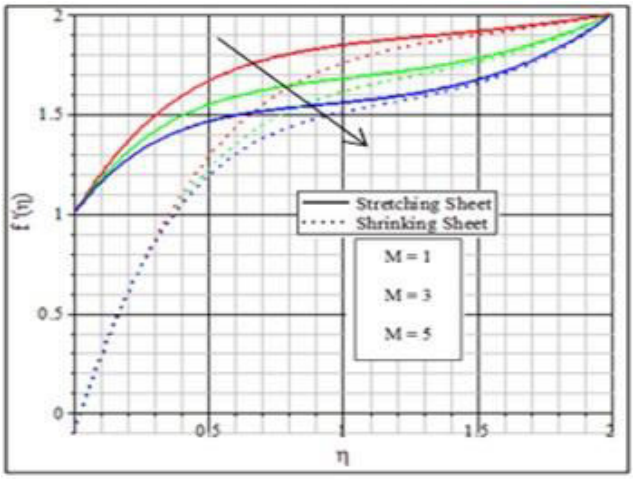

Figure-5. Magnetic effects on velocity profiles over Cu-fresh water (Pr =6.2, ϕ=0.2, Gr=3, K =0.1, S = -1, λ =0.1, N = 1, Ec =0.2).

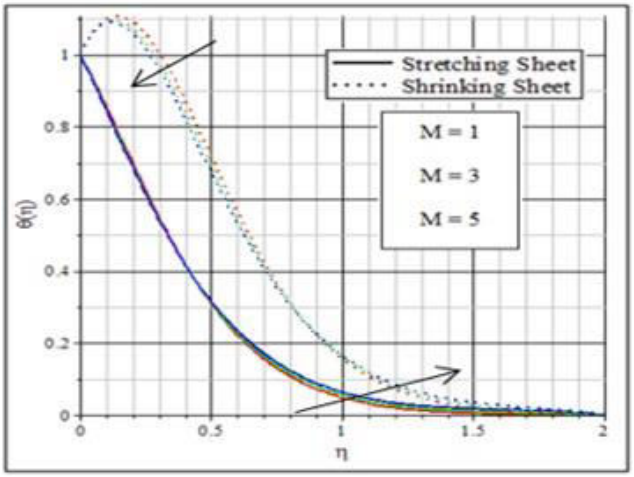

Figure-6. Magnetic effects on temperature profiles over Cu-sea water (Pr =6.2, ϕ =0.2, Gr=3, K =0.1,S= -1, λ = 0.1,N =1, Ec =0.2).

The application of M to an electrically conducting fluid produces a dragline force which causes deceleration in the temperature. Physically, it is interesting to note that the thermal boundary layer thickness of the sea water based copper nanofluids increases significantly as compared to that of the Cu-fresh water because of Cu-sea water has high thermal conductivity. These results clearly demonstrate that the combined effect of thermal radiation with magnetic field can be used as a controlling factor of the flow and heat transfer characteristics because of the thermal conductivity of Cu-sea water and Cu-fresh water.

The effect of heat source (λ) on velocity profiles in the presence of injection over Cu-sea water and Cu-fresh water nanofluids in shrinking and stretching surfaces is shown in Figure-8 and Figure-9. In case of injection velocity on boundary layer, the velocity distribution of nanofluids increases with increase in heat source. Figure-8 and Figure-9., the velocity gradient for higher values that is λ = 4, are very less for both shrinking and stretching surfaces and also differences in magnitude of velocity for λ = 4 is high when compared with velocity profiles for λ = 0.5 and λ = 2.

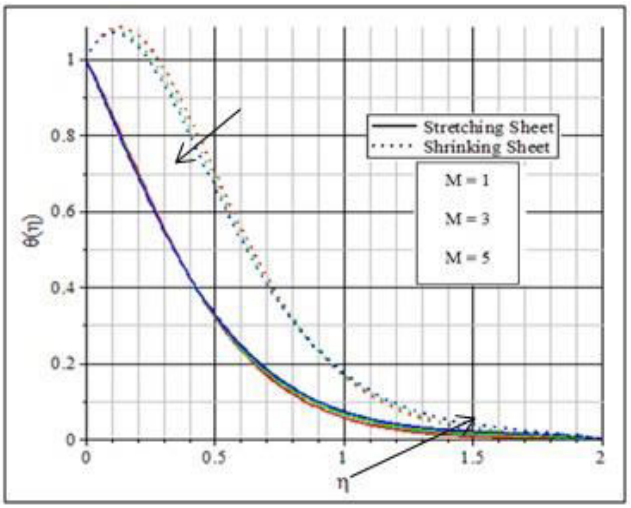

Figure-7. Magnetic effects on temperature profiles over Cu-fresh water (Pr =6.2, ϕ=0.2,Gr=3,K =0.1,S= -1,λ =0.1,N=1,Ec=0.2).

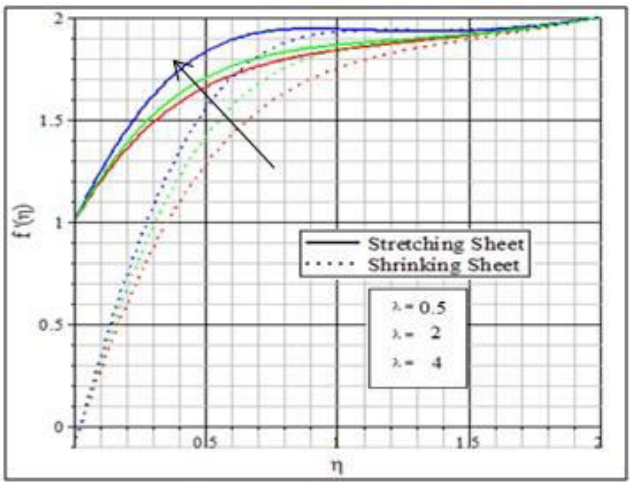

Figure-8. Heat source on velocity profiles over Cu-sea (Pr = 6.2, ϕ= 0.2, Gr= 3, K = 0.1, S = -1, N = 1, Ec = 0.2, M = 1).

In Figure-8 and Figure-9., for high values of λ, in shrinking surfaces the velocity profiles when the flow is nearer to momentum boundary layer, the velocity gradient increases, as the velocity profile becomes $f'(\eta)=0$ at η = 0.02. The effect of λ, in case of injection, velocity distribution in stretching and shrinking surfaces is similar for both Cu-sea water and Cu-fresh water nanofluids.

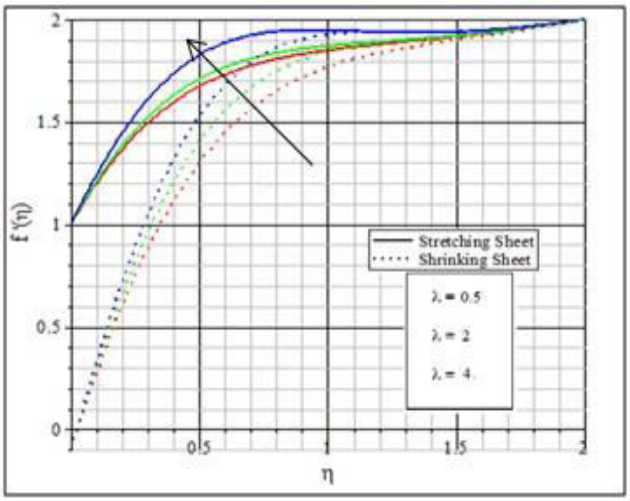

Figure-9. Heat source on velocity profiles over Cu-fresh water (Pr = 6.2, ϕ= 0.2, Gr= 3, K = 0.1, S = -1, N = 1, Ec = 0.2, M = 1).

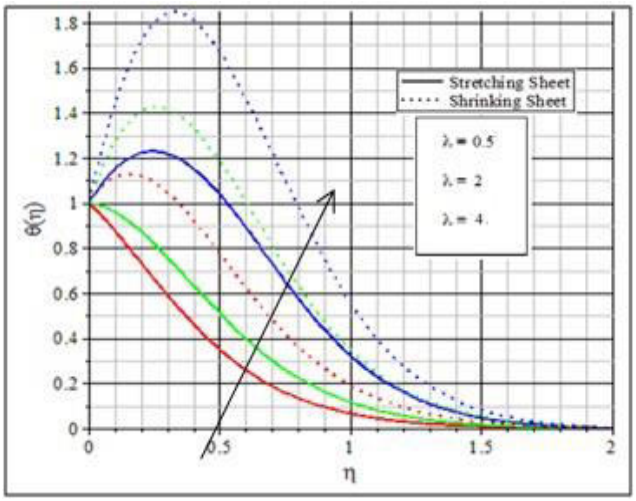

Figure-11. Heat source on temperature profiles over Cu-fresh water (Pr = 6.2, ϕ= 0.2, Gr=3,K=0.1, S = -1,N = 1,Ec = 0.2,M = 1).

Figure-10 and Figure-11 the temperature profiles for different values of λ, is analyzed in the presence of injection. Figure-10 and Figure-11., the temperature profiles increases for increase in λ for both shrinking and stretching surfaces in the presence of injection. Magnitude of temperature profiles of Cu-sea water over shrinking and stretching surfaces is more than that of Cu-fresh water in the presence of injection. For higher values of λ, peak formation in temperature is observed in both shrinking and stretching surfaces.

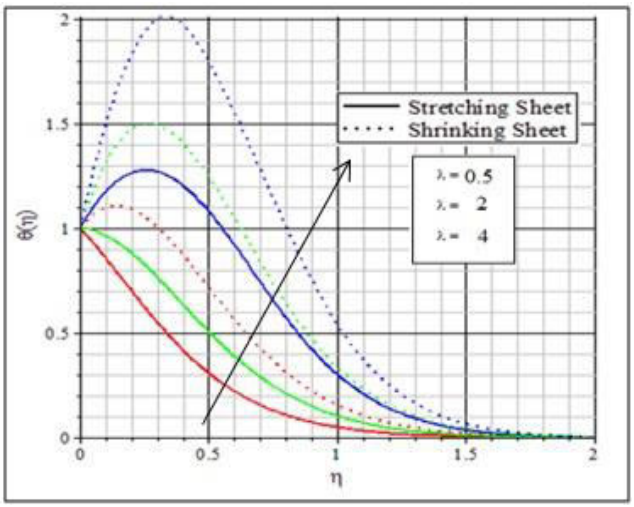

Figure-10. Heat source on temperature profiles over Cu-sea water (Pr = 6.2, ϕ=0.2, Gr=3,K = 0.1, S = -1,N = 1,Ec = 0.2, M = 1).

Figure-12 and Figure-13., depicts the influence of thermal radiation (N) on velocity profiles on Cu-sea water and Cu-fresh water nanofluids in the presence of injection respectively. Velocity profiles show small deviation for increase in N. Velocity profiles are retarded more because of the presence of injection. In injection, the velocity changes for different values of N becomes very less when it is very close to momentum boundary layer and as the nanofluids move away from the boundary layer that is beyond η = 0.8, velocity profiles in stretching surfaces show mild increase with increase in N.

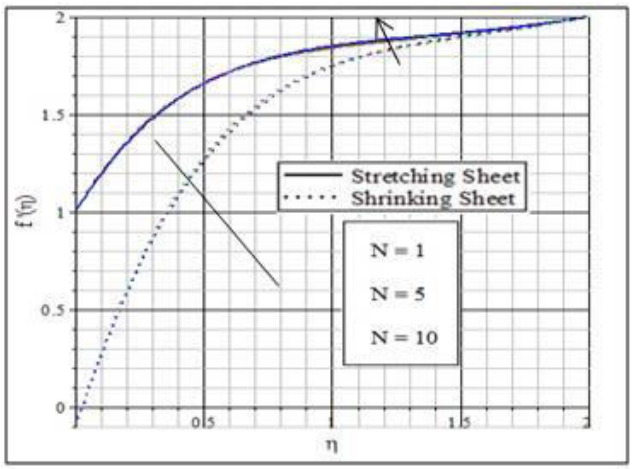

Figure-12. Thermal radiation on velocity profiles over Cu-sea water (Pr =6.2, ϕ= 0.2,Gr=3, K =0.1,S = -1, λ = 0.1,Ec = 0.2,M = 1).

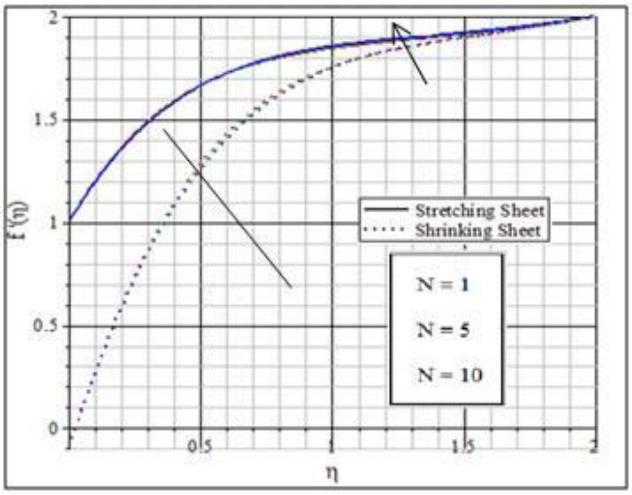

Figure-13. Thermal radiation on velocity profiles over Cu-fresh water (Pr =6.2, ϕ= 0.2,Gr=3,K=0.1, S= -1, λ= 0.1, Ec=0.2,M =1).

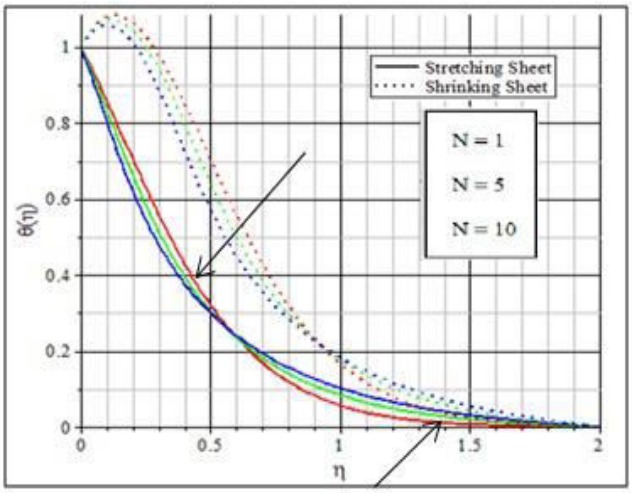

Figure-15. Thermal radiation on temperature profiles over Cu-fresh water (Pr =6.2,ϕ= 0.2,Gr=3,K=0.1,S= -1,λ=0.1,Ec=0.2, M =1).

The temperature profiles of Cu-sea water and Cu-fresh water nanofluids for different values of N in the presence of suction and injection velocity on the surfaces is shown from Figure-14 and Figure-15. The temperature profiles of stretching and shrinking surfaces decrease as the flow is near the thermal boundary layer and increase when they move out of the influence of boundary layer. Temperature profiles of stretching and shrinking surfaces is $\theta(\eta) > 0.3$ at $\eta = 0.5$ in case of injection velocity on the boundary layer. Temperature profiles tends to zero at $\eta = 2$ in the presence of injection. Cu-sea water and Cu-fresh water nanofluids show similar behavior in the presence of injection except when nanofluid flow is close to thermal boundary layer, the profile for N = 10 is $\theta(\eta) > 1.1$ for Cu-sea water but Cu-fresh water nanofluid show temperature profile $\theta(\eta) < 1.1$.

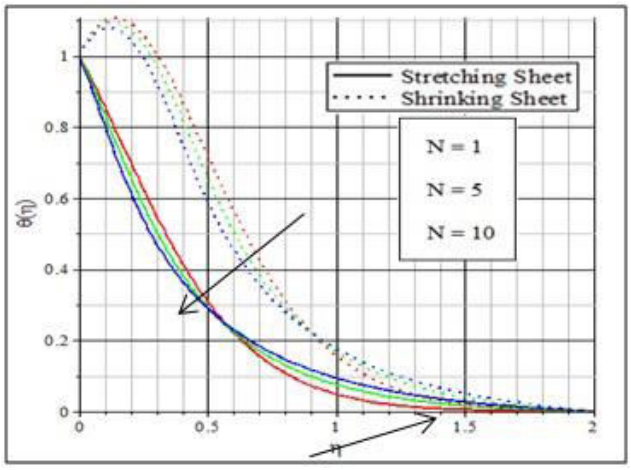

Figure-14. Thermal radiation on temperature profiles over Cu-sea water (Pr=6.2,ϕ= 0.2,Gr=3,K=0.1,S=-1,λ=0.1,Ec =0.2, M=1).

Figure-16 and Figure-17., present the velocity of Cu-fresh water and Cu-sea water in the presence of injection under the effects of Grashof number (Gr). Velocity profiles in shrinking surfaces is lower than the velocity in stretching surfaces. Meaning that the nanofluid flow over shrinking surfaces are retarded more than nanofluid flow in stretching. Velocity profiles are increasing for increasing Gr in both the nanofluids. Similar profiles are obtained in both nanofluids in the presence of injection.

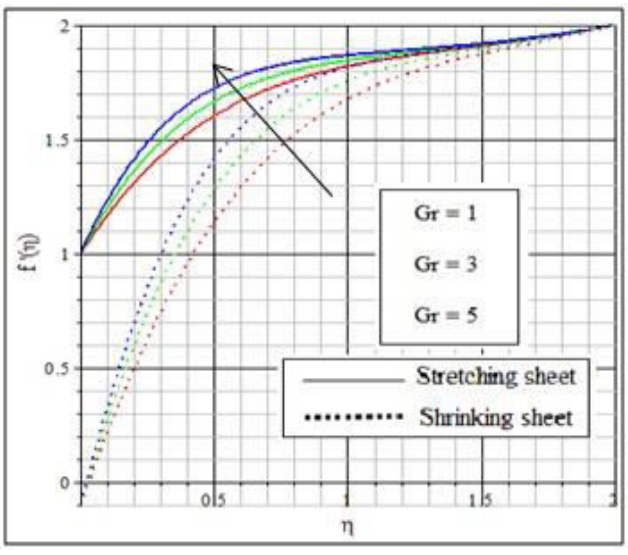

Figure-16. Grashof number on velocity profiles over Cu-sea water (Pr=6.2, ϕ=0.2, K =0.1,S= -1,λ=0.1,N=1,Ec=0.2, M=1).

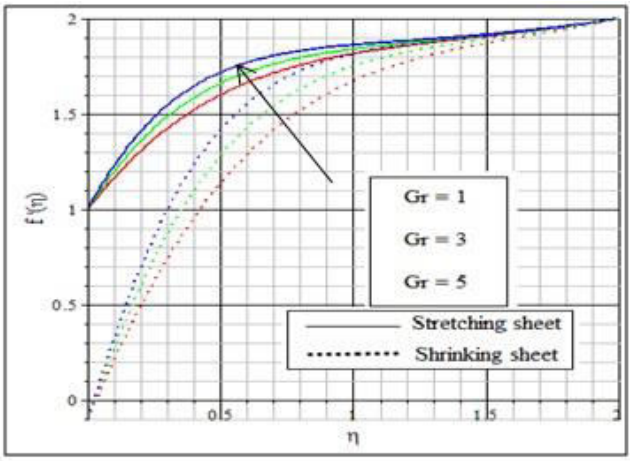

Figure-17. Grashof number on velocity profiles over Cu-fresh water (Pr = 6.2, ϕ= 0.2,K =0.1,S = -1, λ =0.1,N=1,Ec=0.2, M=1).

Figure-18 and Figure-19., presents the Cu-sea water and Cu-fresh water nanofluids' behavior of temperature for various values of Gr. Stretching surfaces in the presence of injection, the temperature profiles overlap into one profile when the flow is close to thermal boundary layer. When the nanofluids flow is beyond η = 0.4, temperature distribution shows a decrease for increase in Gr. The temperature profiles forms a peak near the surfaces as per boundary layer concept. In stretching surface with the influence of injection, temperature distribution increases until η < 0.4 with increase in Gr, beyond η > 0.4, the temperature starts to decrease slowly and tends to zero at η = 2.

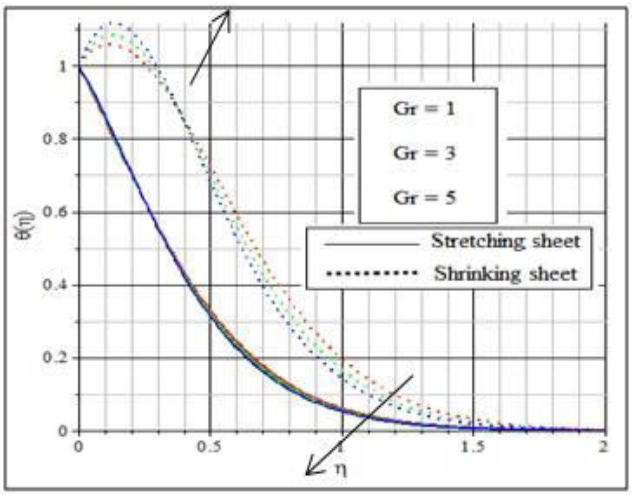

Figure-18. Grashof number on temperature profiles over Cu-sea water (Pr =6.2, ϕ=0.2, K=0.1,S= -1, λ = 0.1,N =1,Ec=0.2, M=1).

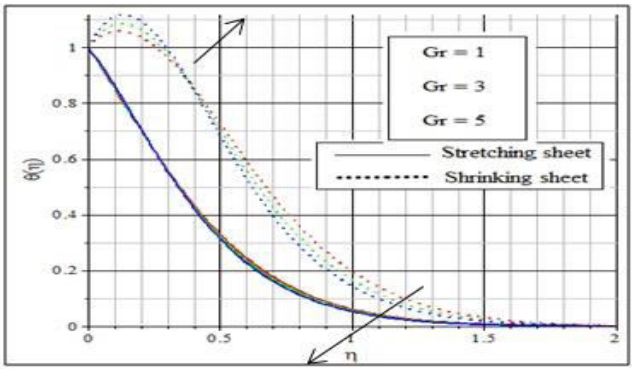

Figure-19. Grashof number on temperature profiles over Cu-fresh water (Pr =6.2, ϕ= 0.2,Ec=0.2,K =0.1,S= -1,λ=0.1,N=1, M=1).

Figure-20 and Figure-21., shows the velocity distribution over Cu-sea water and Cu-fresh water for Eckert number (Ec) in the presence of both injection. In Figure-20 and Figure-21., in the presence of injection, the velocity profiles of stretching surfaces increases with increase in Ec. In shrinking surfaces, the velocity profiles increases with increase in Ec in the presence of injection. In the presence of injection, the velocity profiles are below θ(η)=1.5. For different values of Ec, Cu-seawater and Cu-fresh water nanofluids over shrinking surfaces show similar velocity profiles in the presence of injection.

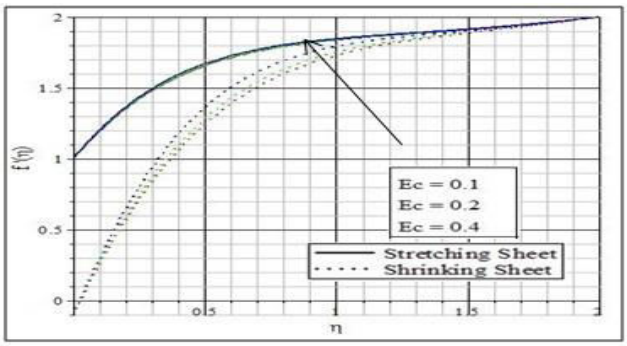

Figure-20. Eckert number on velocity profiles over Cu-sea water (Pr = 6.2, ϕ= 0.2, G = 3, K = 0.1, S = -1, λ = 0.1, N = 1, M = 1).

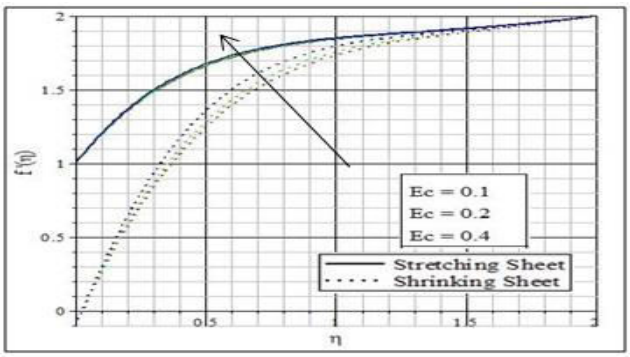

Figure-21. Eckert number on velocity profiles over Cu-fresh water (Pr =6.2, ϕ= 0.2, Gr = 3, K = 0.1,S = -1, λ = 0.1, N = 1,M =1).

From Figure-22. and Figure-23., shows the influence of Eckert number (Ec) on temperature profiles of Cu-sea water and Cu-fresh water nanofluids. Eckert number is a parameter of viscous dissipation. Temperature profiles in shrinking surface shows peak formation but quite opposite results is obtained in the presence of stretching surface as there is no peak formation. The explanation for such behavior is that, when fluid is sheared there is a frictional energy loss and this energy loss is known as viscous dissipation. The energy loss is converted into internal energy of the fluid that corresponds to the rise in temperature. Temperture profiles from Cu-sea water has good results than the Cu-fresh water nanofluid. The explanation for such behavior is that, specific capacity at constant presure (C_p) is high for fresh water compared to sea water as shown in Table-2.2. From $Ec = \frac{{u_w}^2}{C_p \Delta T}$, higher the value of specific heat capacity(C_p) lesser the effect of Eckert number. Thus, Eckert number has more effect on Cu-sea water nanofluid and tends to increase the internal energy causing slight rise in temperature which is evident from Figure-22. and Figure-23. The effect of Eckert number is experienced from a distance from the boundary layer and tends to zero at η = 1.6 (stretching surface) and at η = 1.8 (shrinking surface).

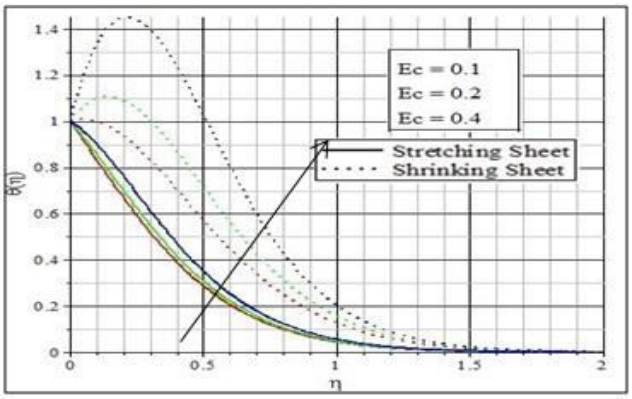

Figure-22. Eckert number on temperature profiles over Cu-sea water (Pr =6.2, ϕ= 0.2, Gr=3, K = 0.1,S = -1, λ = 0.1, N = 1, M = 1).

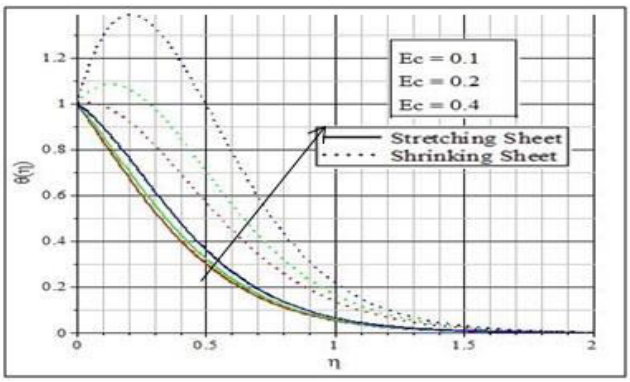

Figure-23. Eckert number on temperature profiles over Cu-fresh water (Pr =6.2, ϕ= 0.2, Gr =3, K = 0.1,S = -1, λ = 0.1, N=1, M =1).

Though there are similar work, but in the present research on heat transfer behavior of fresh water based nanofluids is compared with sea water based nanofluids in stagnation-point flow over porous surface and their performance is studied. The effect of injection factor is studied exclusively. From this study we conclude that, the sea water based nanofluid performance is efficient in stagnation-point flow over porous surfaces and high heat transfer characteristic is obtained in sea water based nanofluid and hence the fresh water based nanofluids can be effectively replaced by sea water based nanofluids in applications which is using stagnation-point flow over stretching or shrinking porous surfaces.

CONCLUSIONS

The main objective of this research is to find out the heat transfer characteristics of the different nanofluids in stagnation-point flow and thermal conductivity enhancement of nanofluids for various parameters such as magnetic field, Thermal radiation, heat source, Eckert number, grashof number in the presence of injection. Even though researches are carried all over the world to use sea water for cooling purposes, there is no research on nanofluids, taking sea water as base fluids. The nanofluids using fresh water and sea water as base fluid are taken into consideration and found that heat transfer efficiency is high in case of sea water based nanofluids. This data are very useful in the consideration of manufacturing sea water based nanofluids for cooling purposes.

ACKNOWLEDGEMENTS

The work was partly supported by Universiti Tun Hussein Onn Malaysia, Johor, Malaysia, under the Short Term Grant Scheme Vot.no. 1289.

REFERENCES

[1] Choi, S., 1995. Enhancing thermal conductivity of fluids with nanoparticle, development and applications of non-Newtonian flow, Fluids Engineering Division, 231, 99–105.

[2] Daungthongsuk, W. and Wongwises, S., 2007. A critical review of convective heat transfer nanofluids, Renewable Sustainable Energy Rev., 11, 797–817.

[3] Trisaksri, V. and Wongwises, S., 2007. Critical review of heat transfer characteristics of nanofluids, Renewable Sustainable Energy Rev., 11, 512–523.

[4] Khanafer, K., Vafai, K. and Lightstone, M., 2003. Buoyancy-driven heat transfer enhancement in a two-dimensional enclosure utilizing nanofluids, Int. J. Heat Mass Transfer, 46, 3639–3653.

[5] Oztop, H.F. and Abu-Nada, E., 2008. Numerical study of natural convection in partially heated rectangular enclosure filled with nanofluids, Int. J. Heat Fluid Flow, 29(5), 1326–1336.

[6] Andersen, D.V.B., 2004. Sea water cooling, Danish board of district heating, 1.

[7] Hamad, M.A.A. and Ferdows, M., 2011. Similarity solution of boundary layer stagnation-point flow towards a heated porous stretching sheet saturated with a nanofluid with heat absorption/generation and suction/blowing: a lie group analysis, Commun. Nonlinear Sci. Num. Simulation, 17, 132–140.

[8] Mahapatra, T.R. and A.S. Gupta, 2001. Magnetohydrodynamics stagnation-point flow towards a stretching surface, Acta Mechanica, 152(1-4), 191–196.

[9] Mahapatra, T.R. and Gupta, A.S., 2002. Heat transfer in stagnation-point flow towards a stretching sheet, Heat Mass Trans., 38, 517–521.

[10] Ishak, A. and Nazar, R., 2008. Uniform suction/blowing effect on flow and heat transfer due to a stretching cylinder, Appl. Math Model., 32(10), 2059–2066.

[11] Pawlowicz, R. 2013. Key physical variables in the ocean: temperature, salinity, and density, Nature Education Knowledge, 4(4) 13.

[12] Sharqawy, M.H., Lienhard, J.H.V. and Zubair, S.M., 2010. Thermophysical Properties of Seawater: A Review of Existing Correlations and Data, Desalination and Water Treatment, 16, 354–380.

[13] Pal, D., Mandal, G. and Vajravelu, K., 2014. Flow and heat transfer of nanofluids at a stagnation point flow over a stretching/shrinking surface in a porous medium with thermal radiation, Appl. Math Comp, 238, 208–224.

[14] Hamad, M.A.A. and Pop, I., 2010. Scaling transformations for boundary layer flow near the stagnation-point on a heated permeable stretching surface in a porous medium saturated with a nanofluid and heat generation/absorption effects, Trans. Porous Medium, 87, 25–39.